Water Splitting Activity of Oxygen-Containing Groups in Graphene Oxide Catalyst in Bipolar Membranes

Rodrigo J. Martínez and James Farrell

[a]Department of Chemical and Environmental Engineering
University of Arizona
1133 E James E. Rogers Way
Tucson, AZ 85721
*Corresponding author: J. Farrell (farrellj@email.arizona.edu)

Abstract

Graphene oxide (GO) is a very effective catalyst for splitting water into H^+ and OH^- ions in bipolar membranes. However, the mechanisms responsible for GO's high catalytic activity for water splitting are not understood. This research investigated the catalytic activity of oxygenated functional groups in GO for proton acceptance and proton release reactions at electric field intensities between 0 and 2.5 x 10^9 V/m. Møller-Plesset second order perturbation method (MP2) simulations were performed to calculate the activation barriers for water splitting catalyzed by: 1) a hydroxyl group attached to the middle of a phenyl ring, 2) a hydroxyl group attached to the edge of a phenyl ring; 3) a carboxylate group attached to the edge of a phenyl ring, 4) an epoxide group and 5) two different carbonyl groups. The catalytic activity of sites on GO was compared with that for a model tertiary amine catalyst, which are commonly used in bipolar membranes. The relative catalytic activity for the functional groups on GO was independent of the electric field intensity and dielectric constant. The catalytic activity for accepting a proton was linearly correlated with the pK_a of the functional group. The catalytic activity for releasing a proton showed an inverse linear correlation with the site pK_a value. For catalyzed water splitting, an electric field of 10^9 V/m reduced activation barriers for the rate limiting step by an average of 9.5 kcal/mol. The edge carboxylate site had the highest catalytic activity for water splitting, and had activation barriers that were 0.2 to 0.4 kcal/mol higher than trimethylamine for the rate limiting step. This suggests that the high catalytic activity of GO results from a high catalytic site density, as opposed to a chemical effect.

Keywords

Bipolar membranes, water splitting, graphene oxide, computational chemistry

1. Introduction

Bipolar membranes (BPM) are used in a wide variety of industrial process to produce acids and bases from the dissociation of water promoted by an electric field. Industrial applications include: deacidification of wine and fruit juices, recovery of organic acids from fermentation broths, reconcentration of diluted acid and caustic solutions, pH adjustment in water treatment processes, and solar water splitting [1–3]. BPMs are three layer composites consisting of a cation exchange membrane, an anion exchange membrane, plus a thin catalyst layer between the two membranes. When placed in an electrodialysis cell with electrodes polarized as in Figure 1, mobile counter ions are drawn out of the bipolar membrane until a critical voltage is reached that commences water splitting in the catalyst layer [4]. Water splitting into H^+ and OH^- ions is promoted by the high electric field in the catalyst layer. Depletion of mobile counter ions at the catalyst/membrane interface can result in electric field values greater than 10^9 V/m [4,5]. The strong electric field promotes both catalyzed and uncatalyzed water dissociation via the second Wien effect [5,6]. Rates of water splitting have been observed to be up to 7 orders of magnitude greater than those in bulk water without an electric field [7].

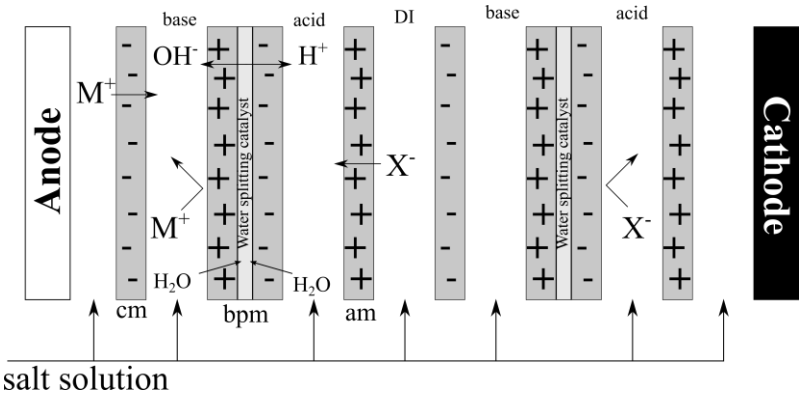

Figure 1. Schematic diagram illustrating the arrangement of anion exchange membranes (am), cation exchange membranes (cm), and bipolar membranes (bpm) for the production of acids and bases from salt solutions.

Simons has proposed that the catalyst enhances the rate of water dissociation by lowering the energy barrier for protonation and deprotonation of weak acids and weak bases via the two reactions [4]:

$$A^- + H_2O \overset{k_1}{\Leftrightarrow} HA + OH^- \text{ or } B + H_2O \overset{k_1}{\Leftrightarrow} BH^+ + OH^- \quad (1)$$

$$HA + H_2O \overset{k_2}{\Leftrightarrow} A^- + H_3O^+ \text{ or } BH^+ + H_2O \overset{k_2}{\Leftrightarrow} B + H_3O^+ \quad (2)$$

where A^- is the conjugate base of weak acid HA, B is a weak base, and k_1 and k_2 are second order rate constants for proton acceptance and proton release [8]. As shown by reactions 1 and 2, a good water splitting catalyst needs to have both proton donor and proton acceptor functional groups. A wide variety of catalysts have been employed in bipolar membranes, including: tertiary amines [6], metal oxides and hydroxides [9], large organic polymers (polyethylene glycol) [10], functionalized polyester [10–13], proteins [14] metal-organic frameworks (MOFs) [15] and graphene oxide [16–19].

Recently, BPMs with graphene oxide (GO) catalysts have been shown to have superior performance compared to a commercial bipolar membrane, requiring 30% less voltage at current densities of industrial interest (e.g., 100 mA/m^2) [16,17]. GO is the product of exposing graphene to high pH and an oxidizing agent. It is typically a macromolecular, one atom thick sheet of sp^2-hybridized carbon. Depending on the preparation method, GO with C:O ratios ranging from 32:1 to 2:1 can be produced [20–22]. The type of oxygen-containing functional groups depends on the

C:O ratio. At C:O ratios less than 16:1, nuclear magnetic resonance and X-ray photoelectron spectroscopy studies have shown that up to 60% of the oxygen is present as carboxylic acids ($R-COOH$) on the edges, and as epoxide groups ($C-O-C$) in the basal plane [20,21]. At C:O ratios higher than 16:1, ~50% of the oxygen is present as hydroxyl groups on the basal plane, ~30% as phenol groups on the edges, and the remainder as epoxides and carboxylic acids. In addition, carbonyl, quinone and lactone functional groups may be present at low concentrations.

The mechanisms responsible for the superior performance of GO catalysts in BPMs are not well-understood. Explanations for the high catalytic activity have included: accelerated water splitting involving hydroxyl and epoxide groups [23,24], high hydrophilicity, high stability at both low and high pH values, and electronic conductivity at high C:O ratios [22]. The mechanisms for water splitting in BPMs are not fully understood, and the electric field intensity and the location where the water splitting occurs are also debatable [5,6,19]. Some investigators have proposed that water splitting occurs only at the interface of the catalyst layer with the monopolar membranes [4], while other investigators have asserted that water splitting occurs throughout the catalyst layer [5].

Recently, quantum chemistry calculations were used to investigate the mechanisms responsible for water splitting and the effects of electric field intensity on the rate enhancement for water splitting [8]. Results from that study showed that there was little enhancement in the rate of water splitting for electric field values less than 10^8 V/m. The electric field was found to lower the activation barriers for water splitting by polarizing the H-O bond in the transition state to a greater extent than in the reactants. The rate enhancement for water splitting was found to be greater than 10^5 for electric field values of 10^9 V/m for a dielectric constant of 78, and as high as

10^7 for a dielectric constant of 20. Quantum chemistry calculations can also be used to investigate the mechanisms responsible for the high catalytic activity of GO for water splitting.

The goal of this study was to investigate possible mechanisms for GO catalyzed water splitting using ab initio calculations. The present study explores the hypothesis that the functional groups in graphene oxide reduce the activation energy of the splitting reaction, which in practice is reflected in higher current densities at constant applied potentials. Towards that end, the catalytic activity of different functional groups on GO were investigated by calculating the activation energies for reactions 1 and 2, with and without an electric field. The catalytic activity for sites on graphene oxide were also compared to those for a model tertiary amine, which are the most common catalysts used in bipolar membranes. The catalytic activities for reactions 1 and 2 were then correlated with pK_a values for different functional groups.

2. Computational methods

The activity of GO as a water splitting catalyst was calculated using the Gaussian18 software package using workstations with 24 and 72 processors. Spin restricted molecular orbital calculations at 25 °C used the Møller-Plesset second order perturbation method (MP2) [25] with the Dunning correlation-consistent basis set, aug-cc-pvtz [26]. In a previous investigation, this basis set was found to yield activation barriers for water splitting that were within 0.5 kcal/mol of the complete basis set limit [8]. Water splitting was simulated using a four water molecule cluster embedded in the Integral Equation Formalism Polarizable Continuum Model (IEF-PCM) [27]. Justification for the use of four explicit water molecules combined with implicit solvation was presented in a previous investigation [8].

For reaction 1, different oxygen containing functional groups on GO were simulated using the structures shown in Figure 2, and included: a deprotonated hydroxyl group attached to the

middle of a phenyl ring ($GO - O^{-}(m)$), a deprotonated hydroxyl group attached to the edge of a phenyl ring ($GO - O^{-}(e)$), a carboxylate group attached to the edge of a phenyl ring ($GO - COO^{-}$), an epoxide group ($GO - O - GO$), a quinone-like group ($GO = O$), and a carbonyl group ($GO - CO$). For comparison purposes, trimethylamine (TMA) was used to simulate a tertiary amine, and a deprotonated penta-2,4-dienoic acid ($R - COO^{-}$) was used as a model aliphatic carboxylate site. Activation energies, associated with proton release (reaction 2), were calculated using protonated structures from Figure 2. Internal energies were calculated as a function of the H-O bond distance for the water molecule undergoing dissociation reaction 1. Likewise, the H-O bond length of the weak acids, or the H-N bond length for the trimethylammonium ion, were used as scanning coordinates for reaction 2. The atomic coordinates of all other atoms were allowed to relax to their minimum energy positions. Structures at the maxima in the energy profiles were then subjected to a Transition State Search using the Berny algorithm [28]. Frequency calculations were performed to verify energy minima and transition sates, and to determine thermal contributions. In order to study the electric field effect on catalyzed water splitting, intensities of 0 (no electric field added) and 0.5, 1 and 2.5 x 10^9 V/m were investigated. The catalysts were not held in fixed orientations or positions. Thus, the catalyst orientation in the electric field, and the orientation of the water dipoles, corresponded to the minimum energy orientations for the water splitting reactions. This is consistent with experimental observations of orientation realignment of graphene oxide layers in strong electric fields [16].

The effect of the number of phenyl rings on catalyst site acidity was investigated by calculating pK_a values for catalytic sites with different numbers of aromatic rings. The pK_a values of the catalyst sites were calculated using the method described by Lian et al. [29], and a value of −265.9 kcal/mol for the aqueous phase proton free energy.

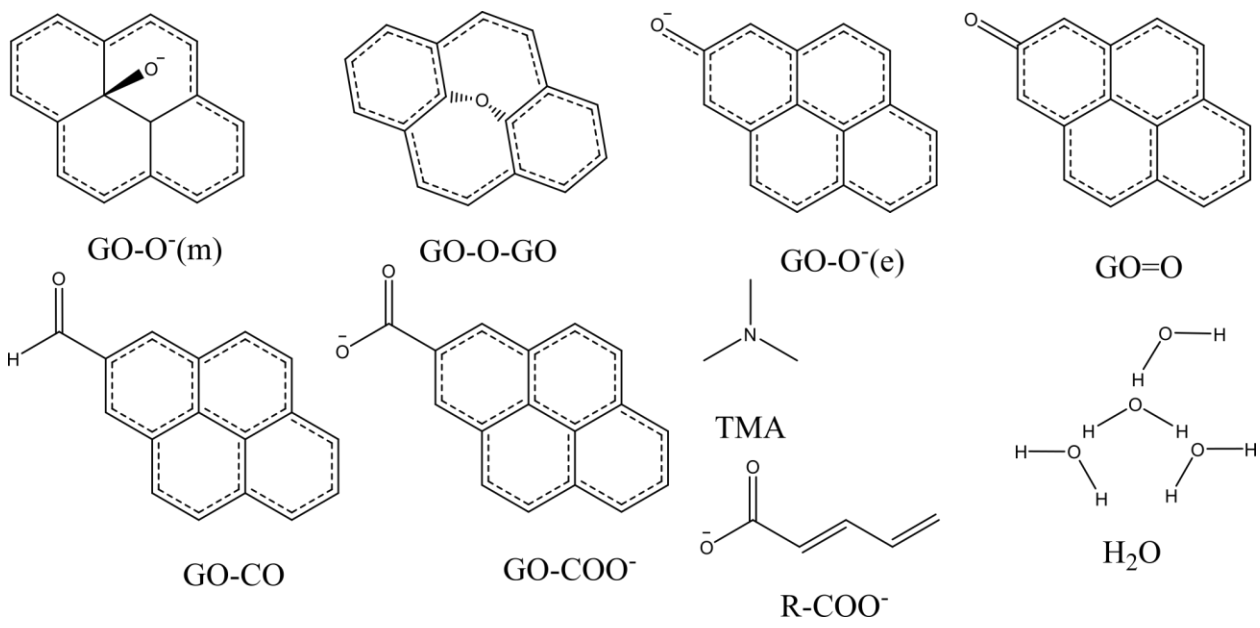

Figure 2. Functional groups used to simulate graphene oxide; H_2O represents the four water molecules cluster used in catalyzed and uncatalyzed calculations.

3. Results

3.1. pKa

Figure 3 shows pK_a values for $GO - O^-(e)$, $GO - O^-(m)$ and $GO - COO^-$ as a function of the number of aromatic rings in the absence of an electric field. For $GO - O^-(e)$, the pK_a decreased as the number of rings increased. Between one and four rings, the pK_a changed from 9.6 to 7.7, whereas between four and six rings the pK_a oscillated within ±0.1 pH units. The compound corresponding to $GO - O^-(e)$ with one aromatic ring is phenol, which has an experimentally measured pK_a of 9.9, which is 0.2 units above the calculated value [29]. The pK_a calculated for TMA was 9.7, which is in agreement within 0.1 pH unit with experimental values

[29]. The pK$_a$ values for $GO - COO^-$ ranged from 4.2 to 4.6, and the value corresponding to one aromatic ring is in agreement with the experimental value of 4.2 for benzoic acid [29]. For $GO - O^-(m)$ to be in the center of the rings, the fewest number of rings possible was three. In this case the pK$_a$ varied between 13.6 and 13.8. The trends in pK$_a$ values showed that starting from four conjugated rings, increasing the number of rings made only small differences on the proton accepting properties of the graphene oxide fragments. Thus, the simulations for the water splitting reactions were made using four rings. In the presence of explicit water molecules, the geometry minimization of the protonated epoxide group resulted in deprotonation and formation of H_3O^+. The pK$_a$ in this case was calculated using only implicit solvation. The pK$_a$ values for $GO - O - GO$, $GO - CO$, and $GO = O$ were below zero. This was expected since the protonated structures were not stable. A list of the pK$_a$ values for the catalyst sites is shown in Table 1.

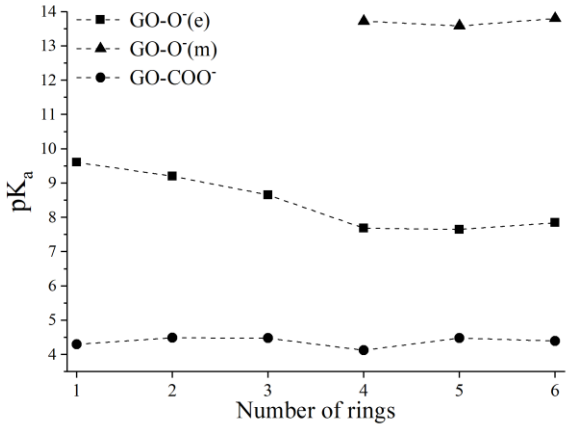

Figure 3. pK$_a$ values for three different oxygen-containing functional groups as a function of the number of aromatic rings.

The presence of an electric field with E=10^9 V/m lowered the pK_a values by 1.7 to 7.3 units. This is consistent with the second Wien effect whereby weak acids undergo increased dissociation in the presence of an electric field [4].

Table 1. pKa values for catalytic sites with electric field intensities of 0 and 10^9 V/m.

Site	**pK_a**	
	0 V/m	10^9 V/m
$GO-O-GO$	-11.7	-16.4
$GO-CO$	-3.0	-7.3
$GO=O$	-2.4	-6.8
$GO-COO^-$	4.1	-3.2
$GO-O^-(e)$	7.7	5.0
$GO-O^-(m)$	13.7	11.7
$R-COO^-$	4.7	-2.1
TMA	9.7	7.7

3.2. Activation energies

Energy profiles for reaction 1 as a function of the H-O bond distance for catalyzed and uncatalyzed reactions for electric field intensities of 0 and 10^9 V/m are shown in Figure 4. The zero of the energy scale was taken as the geometry optimized reactants before the forced stretching of the H-O bond in increments of 0.1 Å. Activation energies are given by the energy differences between the reactants and the optimized transition states. In the absence of an electric field, there were no maxima in the energy profiles. In this case, the activation barrier was calculated for the H-O distance where the energy gradient had declined to < 0.05 kcal/mol-Å. For the simulations with an electric field (Figure 4b), the decline in energy after the maximum point resulted from interactions of the charged ions with the electric field.

The standard Gibbs free energy of activation (ΔG_a^o) for reaction 1 for each site is listed in Table 2. For uncatalyzed water splitting, the activation barrier without an electric field was 65.5 kcal/mol. An electric field of 10^9 V/m lowered the activation barrier to 58.0 kcal/mol. This decrease in ΔG_a^o of 7.5 kcal/mol corresponds to a factor of $10^{5.5}$ increase in the rate of water splitting. For catalyzed water splitting, the activation barriers ranged from 8.6 to 69.1 kcal/mol for the proton acceptance reaction in the absence of an electric field. The electric field reduced the ΔG_a^o values for reaction 1 between 7.1 and 11.0 kcal/mol, except for both carboxylic acids, where the effect was between 4.2 and 4.6 kcal/mol.

Figure 5 shows the energy profiles for each functional group for reaction 2, in which each site releases the proton back onto a water molecule to form H_3O^+. The epoxide group yielded a H_3O^+ from the energy minimization; thus, no energy profile for this functional group is shown and the activation energy can be assumed as 0. The electric field reduced activation barriers between 8.0 and 13.7 kcal/mol, and the reduction in ΔG_a^o was greater for sites that yielded two charged products, as compared to those yielding H_3O^+ and an uncharged site.

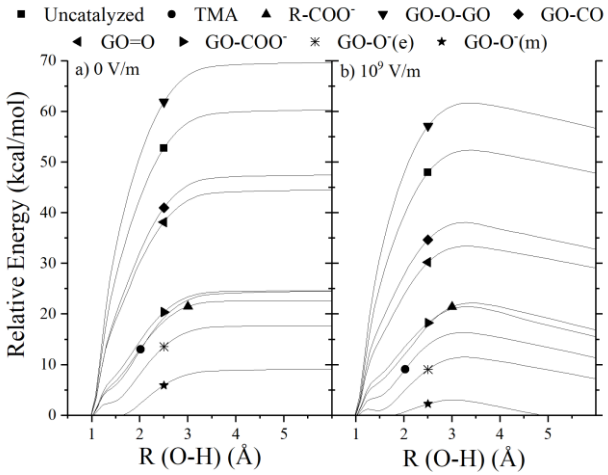

Figure 4. Energy as a function of the H-O bond length for reaction 1 at electric field intensities of 0 and 10^9 V/m. Zero of the energy scale is the geometry optimized starting structures.

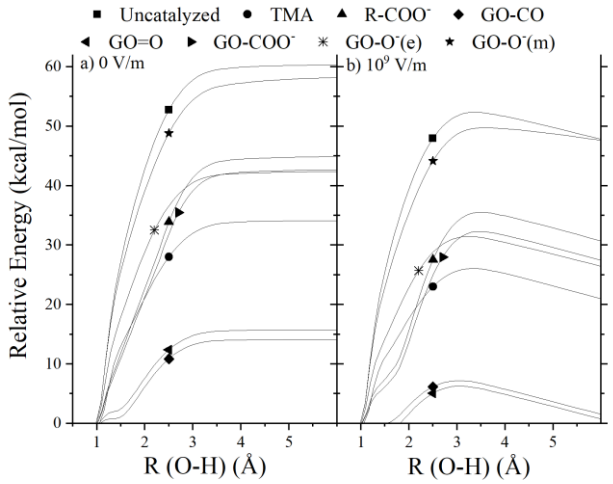

Figure 5. Energy as a function of the H-O bond length (H-N in the case of TMA) for reaction 2 at electric field intensities of 0 and 10^9 V/m. Zero of the energy scale is the geometry optimized starting structures.

Table 2. Activation energies (ΔG_a^o) for uncatalyzed water splitting, and for catalyzed proton acceptance (reaction 1) and proton release (reaction 2) for electric field intensities of 0 and 10^9 V/m. Sites are listed in order of decreasing catalytic activity, defined as the reduction in ΔG_a^o compared to the uncatalyzed reaction, for the rate limiting step. Activation barriers for the rate limiting step are shown in bold.

	$H_2O \rightarrow H^+ + OH^-$			
uncatalyzed	0 V/m (kcal/mol)		10^9 V/m (kcal/mol)	
	65.5		58.0	
	proton acceptance		proton release	
	0 V/m	10^9 V/m	0 V/m	10^9 V/m

TMA	25.5	18.4	**31.1**	**23.1**
$GO-COO^-$	23.0	18.8	**35.4**	**23.3**
$R-COO^-$	22.5	17.9	**37.6**	**23.9**
$GO-O^-(e)$	18.1	10.8	**39.6**	**28.7**
$GO=O$	**42.5**	**31.5**	14.8	5.3
$GO-CO$	**46.6**	**36.0**	11.4	2.4
$GO-O^-(m)$	8.6	0.9	**55.7**	**42.8**
$GO-O-GO$	**69.1**	**60.3**	0	0

The reduction in ΔG_a^o values for reaction 1 by the catalyst sites was linearly correlated with the site's pK_a value in the electric field. The solid and dashed lines in Figure 6 are linear regressions of the data, which had correlation coefficients of 0.969 and 0.909 for electric field intensities of 0 and 10^9 V/m, respectively. For reaction 1, the catalytic effect was greater without an electric field by approximately 7 kcal/mol. For reaction 2, the catalytic effect inversely correlated with the pK_a values of the reaction sites, as shown in Figure 7; the correlation coefficients were 0.975 and 0.903 for electric field intensities of 0 and 10^9 V/m, respectively.

For a two-step process, the reaction with the higher activation barrier will be the rate limiting step for water splitting. This indicates that the most effective catalyst with and without an electric field is TMA, where the rate limiting step was reaction 2. For TMA, the rate limiting step had ΔG_a^o values of 31.1 and 23.1 kcal/mol for field intensities of 0 and 10^9 V/m, respectively. The most effective catalyst site on GO was $GO-COO^-$, which had reaction 2 ΔG_a^o values of 35.4 and 23.3 kcal/mol for field intensities of 0 and 10^9 V/m, respectively. The second most catalytic site on GO was the $GO-O^-(e)$ site, which had reaction 2 ΔG_a^o values of 39.6 and 28.7 kcal/mol for field values of 0 and 10^9 V/m, respectively. In all cases, the relative catalytic activity of the sites was the same in both the presence and absence of the electric field.

The carboxylate group on graphene oxide showed very similar catalytic activity as the aliphatic carboxylate group for both reactions 1 and 2. The slightly greater catalytic activity for reaction 1, and slightly worse activity for reaction 2, by the aliphatic carboxylate versus the $GO-COO^-$ site is consistent with the pK_a trends shown in Figures 6 and 7. Thus, aromatic nature of graphene oxide does not appear to contribute to its catalytic activity.

The effect of the dielectric constant on the catalytic activity are shown in Figure 8 for TMA and $GO-COO^-$. For both sites, the catalytic effect decreased with increasing dielectric constant, but varied by only ~4% for ε values ranging from 20 to 78.5. The effect of the electric field on the catalytic activity of TMA and $GO-COO^-$ is also shown in Figure 8 for ε=50. At all three values of the electric field, the catalytic activity of TMA was greater than that for $GO-COO^-$. Calculations for other sites showed that the relative catalytic activity was independent of the electric field intensity and dielectric constant.

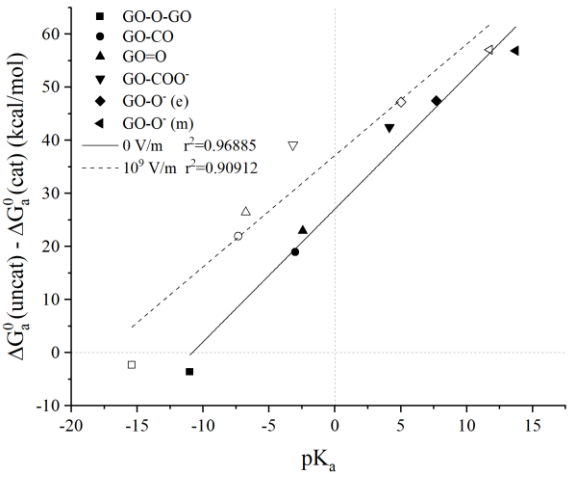

Figure 6. Catalytic activity of each functional group as a function of the pK_a for reaction 1. Solid color symbols represent 0 V/m and open symbols represent 10^9 V/m.

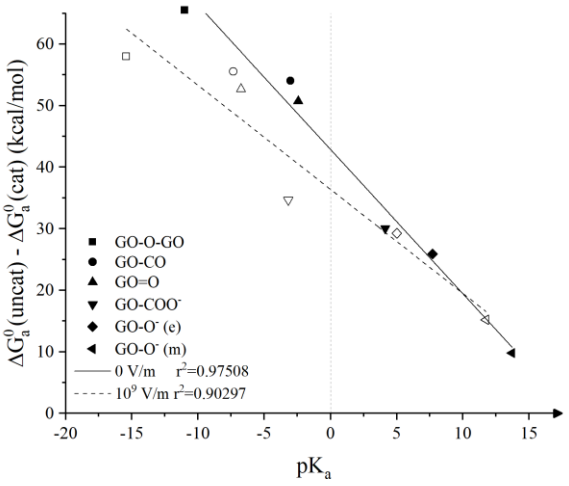

Figure 7. Catalytic activity of each functional group as a function of the pK_a for reaction 2. Solid color symbols represent 0 V/m and open symbols represent 10^9 V/m

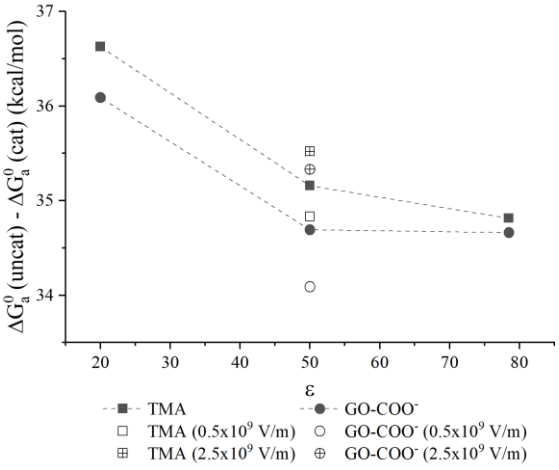

Figure 8. Catalytic activity of TMA and $GO - COO^-$ as a function of the dielectric constant (ε) and electric field intensity. Solid color symbols represent 10^9 V/m, open symbols represent 0.5x10^9 V/m and crossed symbols represent 2.5x10^9 V/m.

4. Conclusions

The activation barriers calculated in this study may underestimate the true activation barriers due to the absence of steric restrictions that may be present in a real bipolar membrane. However, the calculations are useful for determining the relative catalytic activity of different sites, which was independent of electric field intensity and dielectric constant. For the proton accepting reaction, there was a near linear correlation between the catalytic activity and the pK_a of the site, both with and without an electric field. For the proton releasing reaction, there was an inverse correlation between the catalytic activity and the pK_a of the site. The GO site with the best catalytic activity for reaction 1, *GO-CO*$^-$(m), had the worst catalytic activity for reaction 2. Since catalyzed water splitting is a two-step process, the best catalyst will have the lowest activation barrier for the rate-limiting step, which is the step with the highest activation barrier. Thus, the best catalyst sites had good catalytic activity for both reactions.

The GO site with the highest catalytic activity for water splitting was GO-COO$^-$. However, the activity of this site was less catalytic than than the model tertiary amine, TMA. This suggests that the high catalytic activity of GO may result from the high number of reactive sites per unit volume. Previous investigators have reported that the catalytic activity for water splitting increases with increasing GO catalyst loading for thin interlayers, but then decreases as the catalyst layer thickens [17]. This effect has been attributed to two opposing factors: 1) increasing the number of catalytic sites with increasing catalyst loading, and 2) decreasing electric field intensity with increasing interlayer thickness [17,19]. Being a two dimensional material, GO is expected to have a larger number of catalytic sites per unit volume than weak base polymers containing tertiary amine groups. For example, the ion exchange capacity for anion exchange polymers is in the range

of 1.0 - 1.6 meq/g [23,30]. This is lower than that measured for GO. GO nanosheets with a 16:1 carbon oxygen ratio have been reported to have ion exchange capacities as high as 5 meq/g [23,30–32]. Thus, the high catalytic site density on GO allows thin layers to be used, which contributes to higher electric field intensities [5,17], and thus high rates of water splitting [16]. Because the edge carboxylate site was the most catalytically active, small graphene oxide particles with low C:O ratios may be preferred, since they have more carboxylate sites per unit volume compared to larger GO fragments with high C:O ratios.

Acknowledgements

This research was supported by the National Science Foundation Chemical, Bioengineering, Environmental and Transport Systems (CBET) Division through Grant #1604857, and by a fellowship from Consejo Nacional de Ciencia y Tecnología (CONACYT), Mexico to Rodrigo J. Martinez through Grant #409178.

5. References

[1] Y. Chen, J.R. Davis, C.H. Nguyen, J.C. Baygents, J. Farrell, Electrochemical Ion-Exchange Regeneration and Fluidized Bed Crystallization for Zero-Liquid-Discharge Water Softening, Environ. Sci. Technol. 50 (2016) 5900–5907. doi:10.1021/acs.est.5b05606.

[2] M.B. McDonald, J.P. Bruce, K. McEleney, M.S. Freund, Reduced Graphene Oxide Bipolar Membranes for Integrated Solar Water Splitting in Optimal pH, ChemSusChem. 8 (2015) 2645–2654. doi:10.1002/cssc.201500538.

[3] H. Strathmann, Ion-Exchange Membrane Separation Processes, Elsevier, New York, 2004.

[4] H. Strathmann, J.. Krol, H.-J. Rapp, G. Eigenberger, Limiting current density and water dissociation in bipolar membranes, J. Memb. Sci. 125 (1997) 123–142. doi:10.1016/S0376-7388(96)00185-8.

[5] R. Simons, Electric field effects on proton transfer between ionizable groups and water in ion exchange membranes, Electrochim. Acta. 29 (1984) 151–158.

[6] R. Simons, Strong electric field effects on proton transfer between membrane-bound amines and water, Nature. 280 (1979) 824–826. doi:10.1038/280824a0

[7] R. Simons, Preparation of a high performance bipolar membrane, J. Memb. Sci. 78 (1993) 13–23. doi:10.1016/0376-7388(93)85243-P.

[8] R.J. Martinez, J. Farrell, Quantifying Electric Field Enhancement of Water Dissociation Rates in Bipolar Membranes, Ind. Eng. Chem. Res. 58 (2019) 782–789. doi:10.1021/acs.iecr.8b04987.

[9] S.S. Mel'nikov, O.V. Shapovalova, N.V. Shel'deshov, V.I. Zabolotskii, Effect of d-metal hydroxides on water dissociation in bipolar membranes, Pet. Chem. 51 (2011) 577–584. doi:10.1134/S0965544111070097.

[10] A.M. Rajesh, M. Kumar, V.K. Shahi, Functionalized biopolymer based bipolar membrane with poly ethylene glycol interfacial layer for improved water splitting, J. Memb. Sci. 372 (2011) 249–257. doi:10.1016/j.memsci.2011.02.009.

[11] R.Q. Fu, T.W. Xu, G.. Wang, W. Yang, Z.X. Pan, PEG–catalytic water splitting in the interface of a bipolar membrane, J. Colloid Interface Sci. 263 (2003) 386–390. doi.org/10.1016/S0021-9797(03)00307-2.

[12] Y. Xue, T. Xu, R. Fu, Y. Cheng, W. Yang, Catalytic water dissociation using hyperbranched aliphatic polyester (Boltorn® series) as the interface of a bipolar membrane, J. Colloid Interface Sci. 316 (2007) 604–611. doi:10.1016/J.JCIS.2007.08.052.

[13] R.-Q. Fu, Y.-H. Xue, T.-W. Xu, W.-H. Yang, Fundamental studies on the intermediate layer of a bipolar membrane Part IV. Effect of polyvinyl alcohol (PVA) on water dissociation at the interface of a bipolar membrane, J. Colloid Interface Sci. 285 (2005) 281–287. doi:10.1016/J.JCIS.2004.11.050.

[14] M. Manohar, G. Shukla, R.P. Pandey, V.K. Shahi, Efficient bipolar membrane with protein interfacial layer for optimal water splitting, J. Ind. Eng. Chem. 47 (2017) 141–149. doi:10.1016/J.JIEC.2016.11.025.

[15] Q. Wang, B. Wu, C. Jiang, Y. Wang, T. Xu, Improving the water dissociation efficiency in a bipolar membrane with amino-functionalized MIL-101, J. Memb. Sci. 524 (2017) 370–376. doi:10.1016/J.MEMSCI.2016.11.056.

[16] M.B. McDonald, M.S. Freund, Graphene oxide as a water dissociation catalyst in the bipolar membrane interfacial layer, ACS Appl. Mater. Interfaces. 6 (2014). doi:10.1021/am503242v.

[17] H. Wang, F. Ding, G. Jin, C. Li, H. Meng, Ultra-thin graphene oxide intermediate layer for bipolar membranes using atomizing spray assembly, Colloids Surfaces A Physicochem. Eng. Asp. 520 (2017) 114–120. doi:10.1016/j.colsurfa.2017.01.041.

[18] M.B. McDonald, M.S. Freund, P.T. Hammond, Catalytic, Conductive Bipolar Membrane Interfaces through Layer-by-Layer Deposition for the Design of Membrane-Integrated Artificial Photosynthesis Systems, ChemSusChem. 10 (2017) 4599–4609. doi:10.1002/cssc.201701397.

[19] Z. Yan, L. Zhu, Y.C. Li, R.J. Wycisk, P.N. Pintauro, M.A. Hickner, T.E. Mallouk, The balance of electric field and interfacial catalysis in promoting water dissociation in bipolar membranes, Energy Environ. Sci. 11 (2018) 2235–2245. doi:10.1039/C8EE01192C.

[20] S.-Y. Lee, P. Singh, R.L. Mahajan, Role of oxygen functional groups for improved

performance of graphene-silicone composites as a thermal interface material, Carbon N. Y. 145 (2019) 131–139. doi:10.1016/J.CARBON.2018.12.054.

[21] W. Gao, L.B. Alemany, L. Ci, P.M. Ajayan, New insights into the structure and reduction of graphite oxide, Nat. Chem. 1 (2009) 403–408. doi:10.1038/nchem.281.

[22] F. Kim, L.J. Cote, J. Huang, Graphene Oxide: Surface Activity and Two-Dimensional Assembly, Adv. Mater. 22 (2010) 1954–1958. doi:10.1002/adma.200903932.

[23] Y. Zhang, L. Zou, Y. Wimalasiri, J.-Y. Lee, Y. Chun, Reduced graphene oxide/polyaniline conductive anion exchange membranes in capacitive deionisation process, Electrochim. Acta. 182 (2015) 383–390. doi:10.1016/J.ELECTACTA.2015.09.128.

[24] M.R. Karim, K. Hatakeyama, T. Matsui, H. Takehira, T. Taniguchi, M. Koinuma, Y. Matsumoto, T. Akutagawa, T. Nakamura, S. Noro, T. Yamada, H. Kitagawa, S. Hayami, Graphene Oxide Nanosheet with High Proton Conductivity, J. Am. Chem. Soc. 135 (2013) 8097–8100. doi:10.1021/ja401060q.

[25] C. Møller, M.S. Plesset, Note on an Approximation Treatment for Many-Electron Systems, Phys. Rev. 46 (1934) 618–622. doi:10.1103/PhysRev.46.618.

[26] T.H. Dunning, Gaussian basis sets for use in correlated molecular calculations. I. The atoms boron through neon and hydrogen, J. Chem. Phys. 90 (1989) 1007–1023. doi:10.1063/1.456153.

[27] G. Scalmani, M.J. Frisch, Continuous surface charge polarizable continuum models of solvation. I. General formalism, J. Chem. Phys. 132 (2010) 114110. doi:10.1063/1.3359469.

[28] H.B. Schlegel, Optimization of equilibrium geometries and transition structures, J. Comput. Chem. 3 (1982) 214–218. doi:10.1002/jcc.540030212.

[29] P. Lian, R.C. Johnston, J.M. Parks, J.C. Smith, Quantum Chemical Calculation of pKas of Environmentally Relevant Functional Groups: Carboxylic Acids, Amines, and Thiols in Aqueous Solution, J. Phys. Chem. A. 122 (2018) 4366–4374. doi:10.1021/acs.jpca.8b01751.

[30] Y. Bai, Y. Yuan, Y. Yang, C. Lü, A facile fabrication of functionalized rGO crosslinked chemically stable polysulfone-based anion exchange membranes with enhanced performance, Int. J. Hydrogen Energy. 44 (2019) 6618–6630. doi:10.1016/J.IJHYDENE.2019.01.143.

[31] Z. Hu, Y. Chen, Q. Hou, R. Yin, F. Liu, H. Chen, Characterization of graphite oxide after heat treatment, New J. Chem. 36 (2012) 1373. doi:10.1039/c2nj20833d.

[32] S.M. Hosseini, E. Jashni, M. Habibi, M. Nemati, B. Van der Bruggen, Evaluating the ion transport characteristics of novel graphene oxide nanoplates entrapped mixed matrix cation exchange membranes in water deionization, J. Memb. Sci. 541 (2017) 641–652. doi:10.1016/J.MEMSCI.2017.07.022.